

Simulating molecular conductance using real-time density functional theory

Chiao-Lun Cheng, Jeremy S. Evans, and Troy Van Voorhis

Department of Chemistry, Massachusetts Institute of Technology, 77 Massachusetts Avenue, Cambridge, Massachusetts 02139, USA

(Received 8 May 2006; revised manuscript received 14 July 2006; published 16 October 2006)

We present real-time density functional calculations of finite-bias conductance in a polyacetylene molecular wire. Our approach is based on a novel, efficient method for numerically propagating the time-dependent Kohn-Sham equations in a Gaussian basis. Localized density constraints are used to create an appropriate chemical potential bias that, when released, causes charges to flow from one end of the molecule to the other, generating a current. Our numerical scheme is efficient enough that one is able to perform “brute force” conductance calculations by simply increasing the size of the electron reservoirs and propagating until a reasonable average current can be extracted. We demonstrate the feasibility of this approach on a simple polyacetylene wire. By varying the size of the finite leads and comparing to commonly used nonequilibrium Green’s function calculations, we show that reliable current-voltage curves can be obtained from a finite length of the molecular wire, even though the system never reaches a steady state. Our results indicate that it should be technically feasible to perform the same type of “brute force” simulations on molecular junctions, although it seems unlikely that a true steady state will ever be reached in these cases, due to the greater significance of current fluctuations at low transmittance.

DOI: [10.1103/PhysRevB.74.155112](https://doi.org/10.1103/PhysRevB.74.155112)

PACS number(s): 71.15.Mb, 73.63.-b, 71.15.Pd, 73.43.Cd

INTRODUCTION

There is, at present, a significant body of experimental work on the electron transport properties of individual metal-molecule-metal (MMM) junctions.^{1–24} Much of this work is motivated by the visionary technological goal of developing future computers based on “molecular electronics:” machines whose transistors, wires and memory elements are constructed at the single molecule level.^{25–27} However, from a fundamental perspective, these experiments also form the ideal laboratory for the study of electron transfer kinetics and dynamics on a molecule-by-molecule basis.

The first qualitatively correct picture of elastic electron transport through a junction was provided by Landauer and Büttiker.^{28–32} Here, one assumes that each metal lead is in equilibrium with a bath that has a well-defined chemical potential and can act as a source or sink for electrons. Applying the formalism of scattering theory in the low-bias regime results in a steady-state current that rises rapidly at voltages that correspond to the opening of new quantum conductance channels. In MMM junctions, these quantum channels have the character of molecular resonance states, which therefore leads to a natural interpretation of transport measurements in terms of properties of the isolated molecule.^{33–37}

It has been known for quite some time that one can use the nonequilibrium Green’s function³⁸ (NEGF) to derive an exact Landauer-like expression for electron transport through these MMM junctions.^{39–41} These formulas require as input the full quantum many-body NEGF, which is extremely difficult to obtain exactly for real systems. Hence, there have been a large number of investigations that employ various approximations to the NEGF to predict MMM transport-based on semiempirical,^{42,43} *ab initio*,⁴⁴ density functional,^{45–52} and exactly solvable model Hamiltonians.^{53–55} However, even with this level of sophistication at our disposal, there are several significant discrepancies between experiment and theory for these MMM

junctions—most notably the fact that the best calculations and the best experiments still differ by a factor of ≈ 100 as to the conductance of a simple junction. As a result, the challenge of predicting electron transport through these MMM junctions remains an active area of research.

In recent years, several groups have realized that time-dependent density functional theory (TDDFT) provides the tantalizing possibility of an exact implementation of the NEGF approach. The seminal theorem in this area was presented by Runge and Gross,⁵⁶ who proved that for a given initial electronic wave function $\Psi(0)$, there is a one-to-one mapping between the time-dependent density $\rho(t)$ and the time-dependent potential $v(t)$. By subjecting the MMM junction to an appropriate time dependent potential $V(t)$ —that reflects the fact that the bias is “turned on” at some time—one can use TDDFT to evolve $\rho(t)$, which in turn determines the current between the leads. Since TDDFT gives an in principle exact treatment of electron attached and excited molecular states,⁵⁷ this explicitly time dependent picture does not suffer from any of the deficiencies of the mixed NEGF/DFT formalism. These observations have motivated a number of recent investigations that have outlined the formal basis for TDDFT conduction simulations,^{58–60} the expected impact of existing approximate functionals on the conductance,^{61,62} and practical techniques for studying current flow using real-time TDDFT.^{63–66} The work presented here builds upon the ideas set forth in Refs. 63, 65, and 66.

There are two limitations that have, to date, kept TDDFT from realizing the fullness of its promise in this area. The first is simply the computational burden of simulating these systems in real time. In principle, these junctions should be treated as open systems that can exchange particles with their environment; however, in practice one is usually satisfied with leads that are “large enough” to mimic the infinite-system limit.⁶⁰ Further the simulation must be run “long enough” that an effective steady state is established. A number of studies have shown that TDDFT simulations of

realistic-sized systems (e.g., 50–100 atoms) can now be performed for reasonable amounts of time (e.g., femtoseconds),^{67–71} particularly if one integrates the TDKS equations efficiently.^{72–74} As a result of these advances, it has recently been shown that one can now establish a quasi-steady state in a simple metal wire using TDDFT.⁶⁵

The second limitation that has hindered TDDFT conductance simulations to date is the conceptual challenge of unambiguously associating a voltage bias with a given current-carrying state. In the original Landauer formulation, this problem is solved by assuming that the entire junction is in contact with two reservoirs of noninteracting electrons, in which case the bias is simply the difference between the chemical potentials of the two reservoirs. Similar approximations are invoked in the vast majority of modern theories as well: one either derives the bias from the difference between the Fermi levels of left- and right-moving electrons^{40,42,75–77} or from the differences between the Fermi levels deep in the leads.^{45–52} This is problematic because it is well known that the noninteracting system in KS-DFT is fictitious and orbital energies other than the highest occupied level are meaningless.^{78–81} In order to compute the bias, one invariably takes the difference between the highest level (deep in the lead with higher potential or moving with the current) and some lower level (in the lower lead or moving against the current) which is an uncontrolled approximation. These DFT considerations are entirely distinct from the equally important and less ambiguous task of defining the physical quantity to which an experimental voltage corresponds.

In this paper, we describe the first microcanonical real-time TDDFT calculations of finite-bias conductance in a molecular wire. To begin, we present a family of Magnus propagators for real-time TDDFT simulations in a Gaussian basis. These propagators allow us to take very large (e.g., 0.05 fs) time steps and the presence of a localized basis makes it possible to use hybrid functionals [e.g., B3LYP (Ref. 82)] at essentially no additional cost. Next, we illustrate how this can be used to compute the conductance of a polyacetylene molecular wire. In our simulations, both the bias potential and the current through the wire are computed from fluctuations in the atomic populations. This circumvents the above mentioned ambiguities in the definition of the voltage because the voltage definition is *derived* from the associated current. The resulting voltage bias is similar in spirit to the ideas set forth in Ref. 60 and should reduce to the difference in metal Fermi levels^{45–52} in the appropriate large system, weak interaction limit. By testing the convergence of the calculation with respect to lead size⁵² and comparing with analogous NEGF calculations,⁵⁰ we demonstrate that existing TDDFT technology gives reliable predictions of the average current, particularly at low bias. Our simulations suggest the existence of long-lived current fluctuations in the wire that do not disappear in the limit of large leads. This observation stands in contrast to recent TDDFT simulations on an “atomic” gold wire, which reflect no similar fluctuations.⁶⁵ Further, these results emphasize the differences between truly microcanonical TDDFT simulations and approaches where artificial decoherence is introduced to damp fluctuations and drive the system into a steady state^{64,83} We discuss the magnitude of the current fluctuations in our

simulations, viewed as a special type of conductance noise.^{84–91} For polyacetylene, we show that the transient noise is sub-Poissonian but does not appear to vanish in the limit of large leads. Thus, the system never approaches a microscopic steady state. We conclude with a discussion of the transferability of these results to the case of MMM junctions.

THEORY: TDKS PROPAGATION OF THE DENSITY MATRIX

In the KS formulation, one obtains an effective one particle time-dependent Schrödinger equation (TDSE) for the KS orbitals

$$\mathbf{H}_{\text{KS}}[\rho](t)\psi_i(t) = i\frac{d\psi_i(t)}{dt}, \quad (1)$$

where $\rho(t) \equiv \sum_i^{\text{occ}} |\psi_i(t)|^2$ and the notation $\mathbf{H}_{\text{KS}}[\rho]$ is used to emphasize that the KS Hamiltonian depends on the density. Now, the form of the exact KS effective Hamiltonian is unknown, but high level approximations exist.⁹² Most of these approximations are adiabatic— $\mathbf{H}_{\text{KS}}[\rho](t)$ depends only on the density at time t —and from here onward, we will limit our attention to adiabatic forms. The TDKS equations can be formally integrated to give

$$\begin{aligned} \phi(t+dt) &= \mathbf{U}(t+dt, t)\phi(t), \\ \mathbf{U}(t+dt, t) &\equiv T \exp \left\{ -i \int_t^{t+dt} \mathbf{H}_{\text{KS}}(\tau) d\tau \right\}, \end{aligned} \quad (2)$$

where T is the time ordering operator, ensuring that operators associated with later times always appear to the left of those associated with earlier times. Within the adiabatic approximation⁹³ \mathbf{H}_{KS} takes the form

$$\mathbf{H}_{\text{KS}}(t) = -\frac{1}{2}\nabla^2 + v_{\text{ext}}(t) + v_{\text{Jxc}}[\rho(t)], \quad (3)$$

where v_{ext} is an external potential (including the interaction with nuclei and any electric field) and $v_{\text{Jxc}}[\rho]$ is the combined Coulomb-exchange-correlation potential. The former will typically have explicit time dependence (e.g., through the definition of a time-varying potential) while the v_{Jxc} carries implicit time dependence through $\rho(t)$. The implicit time dependence turns out to be the most challenging aspect of these equations and will be dealt with below.

In what follows, we will use the one-particle density matrix (1PDM) $\mathbf{P}(t)$ rather than the KS orbitals to represent the state of the system. This is slightly more general than the KS formalism, as it allows one to treat the evolution of both pure and ensemble states⁹⁴ as well as allowing one to use density matrix functionals in cases where this is desirable.^{95,96} The evolution of the 1PDM is governed by

$$\mathbf{P}(t+dt) = \mathbf{U}(t+dt, t) \cdot \mathbf{P}(t) \cdot \mathbf{U}^\dagger(t+dt, t). \quad (4)$$

Note that in this case \mathbf{P} is not the 1PDM of the true system, but rather a noninteracting reference system with the same density. In what follows, we use the 1PDM both because the

equations are somewhat more elegant and because, in a Gaussian basis set, the number of nonzero elements eventually scales linearly with system size^{97–99} for large insulating systems. This should ultimately facilitate a linear-scaling implementation of real-time TDDFT.

In a simulation, the total propagation interval is typically divided into many small time steps dt . For each time step there are three primary operations: (1) constructing \mathbf{H}_{KS} , (2) constructing $\mathbf{U}(t+dt, t)$, and (3) evolving the 1PDM using Eq. (4). A sophisticated integration scheme may perform these operations more than once per step. For moderate-sized systems (up to 250 atoms) the computational time in a Gaussian basis is dominated by the first step. Thus, the calculation is primarily accelerated by reducing the number of times one needs to construct \mathbf{H}_{KS} . This is accomplished both by taking longer steps (and thus taking fewer steps for a given simulation time) and by minimizing the number of \mathbf{H}_{KS} builds per step by efficient extrapolation. In our implementation, the remaining operations are all accomplished using standard matrix operations. For large systems, these would need to be replaced with the corresponding sparse matrix operations to obtain a linear-scaling algorithm.¹⁰⁰

MAGNUS PROPAGATORS

The time stepping procedure described above ensures time ordering between consecutive steps, but if we want to take truly long steps, we also need to account for time ordering effects within a single step. This can be accomplished using the Magnus expansion.¹⁰¹ Formally, the propagator can be expressed as the (time-unordered) exponential of a series of nested commutator integrals:

$$\begin{aligned}
 T \exp \left\{ -i \int_t^{t+dt} \mathbf{H}_{\text{KS}}(\tau) d\tau \right\} &= \exp(\hat{\Omega}_1 + \hat{\Omega}_2 + \hat{\Omega}_3 + \dots), \\
 \hat{\Omega}_1 &= -i \int_t^{t+dt} d\tau \mathbf{H}_{\text{KS}}(\tau), \\
 \hat{\Omega}_2 &= \int_t^{t+dt} d\tau_1 \int_t^{\tau_1} d\tau_2 [\mathbf{H}_{\text{KS}}(\tau_1), \mathbf{H}_{\text{KS}}(\tau_2)], \\
 \hat{\Omega}_3 &= i \int_t^{t+dt} d\tau_1 \int_t^{\tau_1} d\tau_2 \int_t^{\tau_2} d\tau_3 \{ \mathbf{H}_{\text{KS}}(\tau_1), [\mathbf{H}_{\text{KS}}(\tau_2), \mathbf{H}_{\text{KS}}(\tau_3)] \\
 &\quad + ([\mathbf{H}_{\text{KS}}(\tau_1), \mathbf{H}_{\text{KS}}(\tau_2)], \mathbf{H}_{\text{KS}}(\tau_3)) \}. \\
 &\quad \vdots
 \end{aligned} \tag{5}$$

Recently, Blanes *et al.*¹⁰² have shown how the wave operators, Ω_i , can be efficiently approximated to order $O(dt^{2N})$ using Gauss-Legendre quadrature. The Ω_1 integral is discretized in the standard way:

$$\int_t^{t+dt} \mathbf{H}_{\text{KS}}(\tau) d\tau \approx \sum_i^N w_i \mathbf{H}_{\text{KS}}(\tau_i) + O(dt^{2N+1}), \tag{6}$$

where w_i and τ_i are the weights and grid points of the quadrature. The surprising fact is that the remaining Ω_i inte-

grals can also be evaluated to $O(dt^{2N})$ using \mathbf{H}_{KS} evaluated at the same grid points, τ_i . For example, to second order,

$$\hat{U}(t, t+dt) = \exp(\hat{\Omega}_1) + O(dt^3), \tag{7}$$

$$\hat{\Omega}_1 = -i\hat{H}(t+dt/2) + O(dt^3) \tag{8}$$

while the final form of the fourth order propagator is

$$\hat{U}(t, t+dt) = \exp(\hat{\Omega}_1 + \hat{\Omega}_2) + O(dt^5), \tag{9}$$

$$\hat{\Omega}_1 = -i[\hat{H}(\tau_1) + \hat{H}(\tau_2)] \frac{dt}{2} + O(dt^5), \tag{10}$$

$$\hat{\Omega}_2 = [\hat{H}(\tau_1), \hat{H}(\tau_2)] \frac{\sqrt{3}dt^2}{12} + O(dt^5), \tag{11}$$

$$\tau_{1,2} = t + \left(\frac{1}{2} \mp \frac{\sqrt{3}}{6} \right) dt. \tag{12}$$

Thus, by evaluating \mathbf{H}_{KS} N times within the timestep interval, we obtain a unitary approximation to $\mathbf{U}(t+dt, t)$ correct to order $2N$.

Predictor corrector. The implicit time dependence of \mathbf{H}_{KS} poses a rather significant problem for Magnus integrators. For example, to obtain $\mathbf{P}(t+dt)$ using the second order algorithm [Eq. (8)] one requires $\mathbf{H}_{\text{KS}}(t+dt/2)$, which depends on the 1PDM at time $t+dt/2$, which is not known. Previous applications of the Magnus propagator to TDDFT (Ref. 74) have used iterative techniques to determine $\mathbf{H}_{\text{KS}}(t+dt/2)$. Unfortunately, this process requires many (e.g., 5–10) \mathbf{H}_{KS} builds per timestep, which significantly slows down our simulations. An alternative is to use a predictor-corrector scheme. (1) One uses extrapolation to predict $\mathbf{H}_{\text{KS}}(t)$ within the interval. (2) An approximate 1PDM evolves under the predicted Hamiltonian. (3) $\mathbf{P}(t)$ is used to construct a corrected $\mathbf{H}_{\text{KS}}(t)$. (4) The corrected Hamiltonian is used to accurately evolve the 1PDM. The predictor step requires *no* new \mathbf{H}_{KS} builds, and is therefore very inexpensive. Further, if the extrapolation is correct to $O(dt^{2N-1})$ then the Magnus propagators described above remain accurate to $O(dt^{2N})$. Now, the predictor step is typically unstable; at long enough time steps any algorithm that predicts the future based solely on the past will fail. However, we find that a balanced predictor-corrector strategy can be generated by using the same Magnus expansion for both predictor and corrector phases of the calculation. In this way we can retain the large radius of convergence of the Magnus expansion¹⁰³ at a very modest cost.

In detail, the second order algorithm is illustrated in Fig. 1. The component steps are as follows.

(1) (Predictor) \mathbf{H}_{KS} matrices stored from previous time steps 1a and 1b are used to extrapolate \mathbf{H}_{KS} matrix 3 to order $O(dt)$: $\mathbf{H}_{\text{KS}}(3) = -\frac{3}{4}\mathbf{H}_{\text{KS}}(1a) + \frac{7}{4}\mathbf{H}_{\text{KS}}(1b)$.

(2) (Predictor) Using 3, the density matrix 2 is propagated to 4 using Eq. (8). This is correct to $O(dt^2)$.

(3) (Corrector) Density matrix 4 is used to compute the \mathbf{H}_{KS} matrix 5.

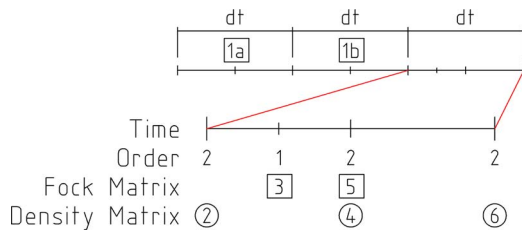


FIG. 1. (Color online) Predictor-corrector routine for the second-order Magnus integrator. The order row shows the time order (in dt) to which the matrices in the same column are correct to.

(4) (Propagation) \mathbf{H}_{KS} matrix 5 is used to propagate the density matrix 2 to density matrix 6 using Eq. (8). This is correct to $O(dt^2)$.

(5) (Update) For the next step, \mathbf{H}_{KS} matrix 1b becomes 1a, \mathbf{H}_{KS} matrix 5 becomes 1b, and density matrix 6 becomes 2. Other matrices are discarded, and the process starts again from step 1.

We have also derived the analogous fourth and sixth order Magnus expansions using MATHEMATICA.¹⁰⁴ Since our results (see below) indicate these propagators are not preferable unless relatively high accuracy is desired, we do not present the (quite involved) fourth, sixth, and eighth order predictor-corrector schemes explicitly.

NUMERICAL VALIDATION

We have implemented the Magnus integrators described above in a local version of the program NWCHEM.¹⁰⁵ For simplicity, we assume the nuclei are fixed and that the time dependence is generated by a (user-specified) sum of pulses of the form

$$\hat{v}_k(r, t) = \alpha_k \hat{O}_k(r) \frac{1}{\sqrt{2\pi\sigma_k}} e^{-(t-t_k)^2/2\sigma_k^2} \cos(\omega_k t + \phi_k), \quad (13)$$

where \hat{O}_k is an arbitrary operator. Our implementation uses the existing optimized subroutines to construct \mathbf{H}_{KS} as needed. Since intuition and numerical experiments dictate that this will be the rate limiting step, this allows us to easily produce efficient, flexible code. Note that, for hybrid functionals such as B3LYP NWCHEM follows the standard prescription of using the Hartree-Fock-like nonlocal form for v_{xc} . This is technically outside the domain of Kohn-Sham DFT—which requires a local v_{xc} —but we do not expect any significant errors from this well-tested approximation. The predictor and propagation phases of the calculation are formulated in terms of standard matrix operations (multiplication, inversion and diagonalization) in the atomic orbital (AO) basis, which are inexpensive for systems with less than a few thousand basis functions. For example, in the AO basis the propagator becomes

$$\mathbf{U}(t) = \exp[\mathbf{S}^{-1}\Omega(t)] = \mathbf{S}^{-1/2} \exp[\mathbf{S}^{-1/2}\Omega(t)\mathbf{S}^{-1/2}]\mathbf{S}^{1/2}, \quad (14)$$

where \mathbf{S} is the AO overlap matrix. $\mathbf{U}(t)$ is computed exactly by (1) computing $\mathbf{S}^{1/2}$ and $\mathbf{S}^{-1/2}$ (only needs to be done once

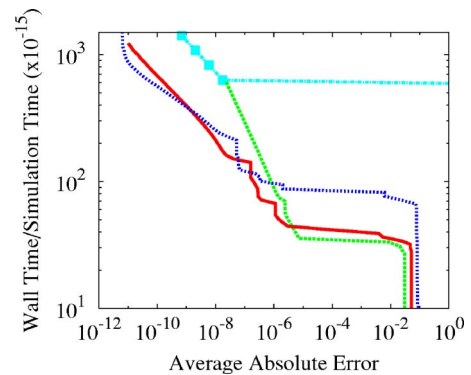


FIG. 2. (Color online) Minimum wall time required to obtain a prescribed average absolute error in the final density matrix of methane (B3LYP/6–31G*, 120 a.u. of propagation) using various approximate propagators: second order Magnus (green dashed), fourth order Runge-Kutta (teal dot-dashed with squares), fourth order Magnus (red solid), and sixth order Magnus (blue dotted).

for all times), (2) diagonalizing $\mathbf{S}^{-1/2}\Omega(t)\mathbf{S}^{-1/2}$, (3) exponentiating $\mathbf{S}^{-1/2}\Omega(t)\mathbf{S}^{-1/2}$ in the eigenbasis, and (4) pre- and post-multiplying the result by $\mathbf{S}^{-1/2}$ and $\mathbf{S}^{1/2}$. There are no approximations due to Chebyshev expansions or Trotter factorizations of the propagator and thus all the Magnus propagators are rigorously unitary.

Our first task is to determine what timesteps are appropriate for these Magnus propagators. The value of having a large critical timestep is perhaps best illustrated by plotting the wall time required to propagate the 1PDM with a given accuracy. In Fig. 2, we present an illustration of this type for methane in a 6–31G* basis¹⁰⁶ using the B3LYP functional.⁸² We begin with the molecule in its ground state and apply a dipole pulse along one of the C_2 axes with a Gaussian envelope in time (intensity $\alpha_k=0.1$, width $\sigma_k=5$, center $t_k=50$, all in a.u.) and evolve the system for 120 a.u. At the end of each simulation, we measure the error

$$\text{Error} = \frac{1}{K^2} \sum_{i,j} |P_{ij}^{\text{exact}}(t_f) - P_{ij}^{\text{approx}}(t_f)|, \quad (15)$$

where K is the number of basis functions and the “exact” density matrix is obtained using sixth order Magnus with a very small time step. It is clear from the figure that for very high accuracy the higher order methods outperform the low-order methods. If one was interested in obtaining near-machine precision results, the high order propagators are the clear choice. However, more typically, we are interested in the most economical way to obtain results of reasonable accuracy (e.g., with errors of order 10^{-4} in the 1PDM). As can be seen in Fig. 2, the low order methods are often more efficient for moderate accuracy. While fourth- and sixth-order Magnus are always more precise than second-order for a fixed timestep, second-order Magnus is often more efficient (i.e., requires the least wall time) due to the fact that it requires one half (one third) as many \mathbf{H}_{KS} builds as fourth- (sixth-) order Magnus. As a result, for moderate accuracy, second-order Magnus can actually be the propagator of choice. We have also compared these Magnus expansions to



FIG. 3. (Color online) Schematic of the source-wire-drain geometry used in the present simulations. The bias is applied to the left and right groups of atoms, which act as a source and drain for electrons, respectively. For different wire lengths (e.g., 50 carbons versus 100) the wire length is kept fixed and the size of the source and sink are varied.

the commonly used fourth-order Runge-Kutta (RK4) integrator. RK4 abruptly diverges even for fairly small time steps of 0.2 a.u., resulting from the loss of normalization in the Kohn-Sham wave functions (see Fig. 2). On the other hand, Magnus integrators are convergent for every time step, and with these larger time steps, Magnus propagators are 15–20 times more efficient than RK4 for these systems. The results from this and other test cases indicate that second-order Magnus with a time step of 1–2 a.u. is usually the most efficient way to propagate the density within an error of 10^{-4} – 10^{-5} .

CONDUCTANCE OF A MOLECULAR WIRE

We now outline how TDDFT can be used to compute the conductance of a short, four-carbon segment of a polyacetylene wire where the role of the reservoirs is played by the semi-infinite left and right strands of the wire. Now, as stated previously, TDDFT is only able to handle the dynamics of closed quantum systems, so we must make a finite model of the infinite wire if we hope to make any progress. We will therefore focus our attention on oligomers of the form $C_N H_{N+1} - C_4 H_4 - C_N H_{N+1}$ (see Fig. 3) with the implicit assumption that N must be chosen “large enough.” Our choice of these model systems is inspired by previous work on short carbon wires embedded in jellium layers.^{35,63} The resulting calculations on these simple wires are intended to illustrate the important points that will arise for more complicated junctions.

We will further restrict our attention to only one particular functional⁸² (B3LYP) and one particular basis set (6–31G*).¹⁰⁶ There are undoubtedly interesting variations on these results with different model chemistries. However, our emphasis here is on the changes that must be applied independent of the model chemistry in order to extract transport properties from the dynamics. Thus B3LYP/6–31G* simply serves as a good model chemistry and could be replaced with any other combination of functional and basis set. Further, since we are interested in treating elastic conduction, the nuclei are held fixed throughout each calculation at their optimal positions at zero bias.

USING A NUMBER BIAS TO DEFINE THE INITIAL CONDITIONS

In the context of this paper, we focus on potential-driven (rather than current-driven) conduction. In this case, there are at least two different prescriptions one can use to simulate

conduction using TDDFT, depending on whether the current is driven by a chemical potential bias (μ) or a voltage bias (V). In the V case, the TDDFT prescription is to begin with the system at equilibrium with no external potential and then turn on a voltage V_L (V_R) in the left (right) lead such that $V = V_L - V_R$. The resulting voltage bias will drive a current from left to right for positive V . The μ case is somewhat more complicated. Here, one considers that the system is connected to two reservoirs (L and R) that are held at constant chemical potential (μ_L and μ_R). If the leads are large enough, this can be accounted for by equilibrating the system with each lead held fixed at its own chemical potential (μ_L or μ_R). Then, at time zero, the constraining chemical potential is removed allowing current to flow from regions of high chemical potential to low. Depending on the experiment, either scheme could be the more appropriate model, but the μ - and V -biased prescriptions tend to give very similar I - V curves.¹⁰⁷ We expect differences to primarily manifest themselves in the distinct transient dynamics of μ - and V -biased junctions¹⁰⁸ and the convergence of the two prescriptions toward the thermodynamic limit. Since both of these issues are germane to the task of making the simulations “large enough” and “long enough” to mimic experiments, we will examine both prescriptions in what follows.

No matter which bias scheme one chooses, there is necessarily some ambiguity about how one defines the potential. The only piece of experimental information we have is that, when averaged over a macroscopic volume deep in the leads, there is a constant shift of the potential on the left relative to the right. This leads to any number of different microscopic potentials that satisfy this condition. Steplike potentials,^{48,65} ramp potentials,^{45,63} and potentials defined in terms of localized orbitals^{47,49,51,52} all give qualitatively similar I - V curves. In this paper, we propose to use atomic Löwdin populations¹⁰⁹ to define the potential in the following way. First, we note that the Löwdin population (N^X) for a given set of atoms (X) can be written as the trace of an operator matrix with the one particle density matrix (\mathbf{P}):

$$N^X \equiv \text{Tr} \mathbf{P} \mathbf{W}^X, \quad (16)$$

where \mathbf{W}^X is given by

$$W_{ij}^X \equiv \sum_{\alpha \in X} S_{i,\alpha}^{1/2} S_{\alpha,j}^{1/2} \quad (17)$$

and the summation runs only over atomic orbitals centered on atoms in the fragment X . It has been shown that \mathbf{W}^X is a projection operator,¹¹⁰ so the atomic populations are always non-negative. Next, we define the bias potentials \mathbf{V}^B ($B = L, R$) to be simply a constant V_B times the appropriate Löwdin operator:

$$\mathbf{V}^B \equiv V_B \mathbf{W}^B. \quad (18)$$

This choice is motivated by previous studies within our group, which show that using this population definition within constrained DFT leads to a consistent treatment of long-range charge transfer excited states^{111,112} and low-lying spin states.¹¹³

Given this definition of the potential, both the μ - and V -biased cases can be simulated using an appropriate time dependent potential $\hat{V}(t)$. For the chemical potential, $\hat{V}(t) = V^B \theta(-t)$, while for the voltage bias, $\hat{V}(t) = V^B \theta(t)$, where $\theta(t)$ is the Heaviside step function. In both cases, the system is equilibrated to the ground state at $t = -\infty$ (or, equivalently, at time $t = -\epsilon$) and then propagated forward in time using TDDFT. Because the system always begins in the ground state, there are no ambiguities about initial wave function dependence in either case. We note that the function used to turn the potential on or off in time is arbitrary. However, the average currents presented below are insensitive to the choice of the switching function as long as $f(t)$ changes from 0 to 1 within ≈ 15 a.u. Slower switching results in a partial depletion of the finite reservoirs before the bias is completely established.

In principle, the current through the device also needs to be defined. In the experiment, the current is measured deep in the leads and in a finite system it is not clear where the dividing surface should be placed in a simulation to best mimic the experiment. However, because we have chosen to define our bias in terms of a particular (albeit arbitrary) population definition, the definition of the current is uniquely determined via the continuity equation

$$\frac{1}{2} \int_L \vec{I} \cdot \vec{n} d\sigma_L - \frac{1}{2} \int_R \vec{I} \cdot \vec{n} d\sigma_R = \frac{d}{dt} \frac{(N^L - N^R)}{2}, \quad (19)$$

where σ_R and σ_L are the surface elements associated with the boundaries of the left and right leads. The left hand side is the current we seek: the average of the current out of the left hand lead (first term) and the current into the right hand lead (second term). The surface implied by the use of Löwdin populations is extremely complicated to define, and hence the left hand side is extremely difficult to evaluate. On the other hand, the right hand side is just the time derivative of the Löwdin populations, easily obtainable from TDDFT. Further, since our bias couples directly to N^L and N^R it is most natural to think of the fluctuations in these variables as generating all the dynamics. For the present study, we use the right side of Eq. (19) to define the current through the junction in our simulations. Indeed, for any given definition of the potential (19) gives a unique prescription for the current through the device region. This equivalence is part of a deep connection between current and number fluctuations in electrical junctions.¹¹⁴

AVERAGE CURRENT

To begin with, we study the molecular wire $C_{50}H_{52}$ under a chemical potential bias. The electronic energy of the molecule is minimized while the left (right) $C_{23}H_{24}$ segments are subject to a bias of $+\mu(-\mu)$ in the Löwdin potential. An example of one such initial state is illustrated in Fig. 4 for a short wire. At time zero, the bias is removed and the electrons are allowed to relax. Figure 5 shows the resulting current at a series of different voltage biases. Several important points follow from this figure. First, even for this wire length, the left and right chemical potentials equilibrate very



FIG. 4. (Color online) Initial density corresponding to a chemical potential bias in polyacetylene. Red indicates charge accumulation and green charge depletion relative to the unbiased ground state. At time $t=0$ the bias is removed and current flows from left to right.

rapidly, as evidenced by the fact that the current pinches off within about 2.5 fs. Second, there is clearly a general trend toward increasing current as we increase the bias, reflecting the current-voltage relationship for this wire. Finally, significant transient current fluctuations (“noise”) hinder the identification of the average current based on in these calculations. The noisiness of the data can be overcome by realizing that experimental measurements are made on a much coarser timescale than the timestep of our simulation. A better approximation to the experimental current can be made by averaging Eq. (19) over a relatively wide time interval Δt :

$$I_{\text{avg}} \equiv \frac{[N^L(t) - N^R(t)] - [N^L(t - \Delta t) - N^R(t - \Delta t)]}{2\Delta t}. \quad (20)$$

This expression physically corresponds to the gedanken experiment where an apparatus with finite time resolution Δt checks the number bias twice in succession and then uses the mean value theorem to approximate the derivative. This process will ignore fluctuations that occur on a time scale faster than Δt resulting in qualitatively smoothed current profiles. Figure 6 shows the transient currents obtained when one applies Eq. (20) (with $\Delta t = 0.36$ fs) to $C_{50}H_{52}$ at various biases. As expected, the transient fluctuations are suppressed and one can now see the earmarks of smoothly increasing current in these molecular wires. It is somewhat remarkable that these molecules are able to attain a quasisteady state so quickly (faster than 1 fs), and similar observations have been made previously for a simple gold wire.⁶⁵ We attribute this fast relaxation in molecular wires to the nearly perfect coupling between the “leads” and the “wire.” Strong system-

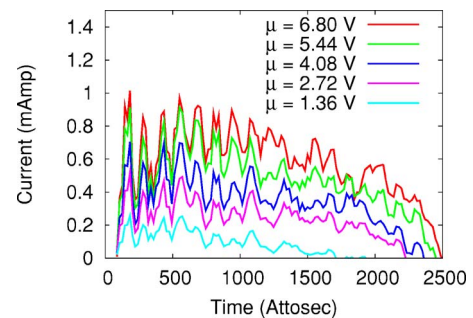


FIG. 5. (Color online) Transient current through the central four carbons in $C_{50}H_{52}$ at a series of different chemical potential biases. There is an increase in current as voltage is increased, along with large, persistent fluctuations in the current. The currents are converged with respect to time step and the apparent noise is a result of physical fluctuations in particle flow through the wire.

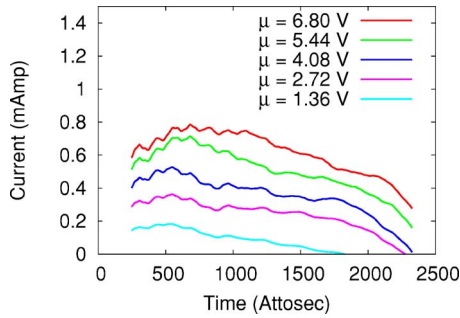


FIG. 6. (Color online) Transient current through the central four carbons in $C_{50}H_{52}$ at a series of different chemical potential biases smoothed over a time window of width $\Delta t=0.36$ fs. The average currents are now more clearly visible. The slow decay of the current at later times results from the partial equilibration of the finite left and right leads.

bath coupling leads to a very short lifetime for transient states and quick relaxation.

If we interpret the maximum smoothed currents in Fig. 6 as the appropriate steady-state current for each voltage, we obtain the current-voltage relation shown in Fig. 7. From this graph it is clear that the current through the wire increases in very nearly linear fashion over a very wide range of voltages. There is a leveling off in current at large voltages that results from an essentially complete depletion of the valence states of the central part of the wire. Perhaps surprisingly, while the conduction is quasi-Ohmic, the conductance is *not* one quantum of conductance ($G_0 \approx 74.5 \mu S$). Instead, the low-bias behavior is better approximated by a conductance of $0.8 G_0$. Initially, one might suspect that this is a finite size effect; that is to say that if the leads were “long enough” the conductance would approach G_0 . To check this we have run similar calculations changing the size of the leads in the wire, keeping our attention on the conductance of the central four carbons. As an example, Fig. 7 also shows a few I - V points for $C_{100}H_{102}$. We have considered only a few voltages because of the increased computational burden per voltage point. How-

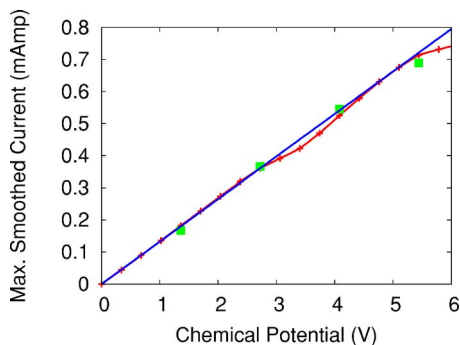


FIG. 7. (Color online) Maximum smoothed current through the central four carbons in $C_{50}H_{52}$ as a function of chemical potential bias (red pluses). For comparison, we also present the analogous result for the central carbons in $C_{100}H_{102}$ (green squares) demonstrating convergence of the calculation with respect to lead size. The blue line is a linear fit to the $C_{50}H_{52}$ data at low bias indicating that polyacetylene is an Ohmic resistor with a conductance of $\approx 0.8G_0$

ever, even this sparse set of data allows us to conclude that the differences between the C_{50} and C_{100} data are quite small and have little influence on the conductance. Thus, our approach of using larger and larger finite systems has indeed converged to the open system limit, but with a finite wire resistance.

In order to understand the origin of the conductance in this wire, we return to the original Landauer picture. Because the “leads” have an essentially perfect connection with the “molecule” in these polyacetylene wires, the appropriate picture involves strong coupling between the leads and the molecule. This coupling *broadens* the molecular levels to the point where the I - V curve becomes featureless. Recall that, in the weak coupling limit, the current displays a staircase structure as a function of bias, and so Fig. 7 should be interpreted as the limiting case where this staircase pattern is “smeared out” yielding a smooth I - V characteristic. Thus, the conductance of the central four carbons should not be viewed as coming from a single quantum state, but from the superposition of a number of broadened states. The numerical value of the conductance thus reflects the density of states available in this wire.

COMPARISON TO NEGF RESULTS

It is important to note that the current-voltage results from the present approach are completely equivalent to the NEGF formalism,⁵⁸ insofar as the dynamics above approximate the true steady state of the infinite system. Therefore, a comparison between DFT-NEGF and real-time DFT predictions of the current voltage curves for polyacetylene provide an additional reality check for these calculations. To this end, we have used the simple scheme of applying a Lorentzian broadening to the leads in order to obtain conductance results out of finite polyacetylene chains.⁵⁰ To be precise, we transform \mathbf{H}_{KS} into the Löwdin orthogonalized basis and partition the molecule in precisely the same manner as in the time dependent simulations. We then add a constant imaginary part $\varepsilon = 0.055$ to the diagonal of \mathbf{H}_{KS} in each lead effectively broadening the lead states and approximating the state continua of infinite wires. The value of ε was chosen to maximize the current making the NEGF current analogous to the time dependent results above (which charted the maximum smoothed current versus voltage). The current is then computed using a previously outlined NEGF technique.⁵⁰ This approach does not compute the current self-consistently, because \mathbf{H}_{KS} is calculated using the equilibrium electron density. However, this simple technique should suffice for the purposes of comparison, particularly at low bias where the self-consistent density should resemble the ground state.

Our NEGF results for $C_{50}H_{52}$ are presented in Fig. 8 along with the real-time TDDFT results from the previous section. Clearly, the two techniques agree near-quantitatively at low bias and give qualitatively similar results at larger biases. Presumably, a large fraction of the difference at large bias can be accounted for by the lack of self-consistency in the NEGF calculations; as the bias increases, the nonequilibrium density will deviate more significantly from the equilibrium result, leading to larger self-consistency corrections.

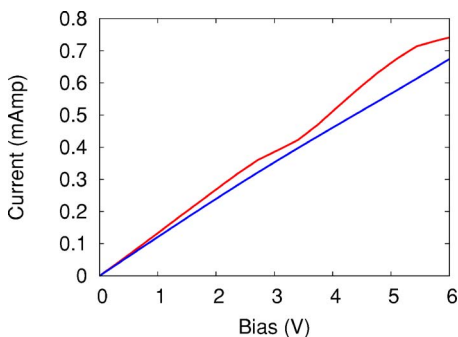


FIG. 8. (Color online) Maximum smoothed current through the central four carbons in $C_{50}H_{52}$ as a function of chemical potential bias using real-time TDDFT (red line) and an NEGF approach described in the text (blue line). The two calculations are nearly identical at low bias and differ somewhat at higher biases due to the lack of self-consistency in the NEGF results.

In any case, taken together these results strongly indicate that our real-time simulations are accessing the open-system limit for this process: the conductance curve does not change appreciably if we increase the lead size (Fig. 7) and the results agree with a simple NEGF calculation (Fig. 8) in the low-bias limit. We therefore conclude that these relatively short wires are capable of mimicking the transport properties that would be observed in a wire attached to much larger (practically infinite) leads. It seems likely that similar conclusions hold for the more experimentally relevant case of molecular junctions, namely, that by simulating the conductance of a molecule attached to large but finite metallic leads it should be technically feasible to approximate the infinite-lead results with a finite system. One thing that will make the latter situation more challenging is the expected relevance of *noise* as discussed below.

VOLTAGE BIASED CASE

The preceding results were all obtained using a chemical potential bias. We have also investigated the effects of using a voltage bias to generate the conductance and find that the results are qualitatively no different. To illustrate this point, the current-voltage plot for $C_{50}H_{52}$ using both μ and V biases is shown in Fig. 9. Clearly, the differences between the two schemes are small until a bias of about 4 V, at which point the voltage biased results show some negative differential resistance. A brief inspection reveals that the plateau at high bias again results from the finite width of the polyacetylene valence band, which apparently has a somewhat larger influence in the voltage biased case.

TRANSIENT CURRENT FLUCTUATIONS

Now, we must stress that the fluctuations in the current shown in Fig. 5 are not numerical noise. Instead these fluctuations reflect the spontaneous, deterministic variation of current in our wire. Further, we have verified that these fluctuations do not appear to be a finite size effect. For example, examining the current fluctuations with larger reservoirs in $C_{100}H_{102}$ one notices that the magnitude of the variations in

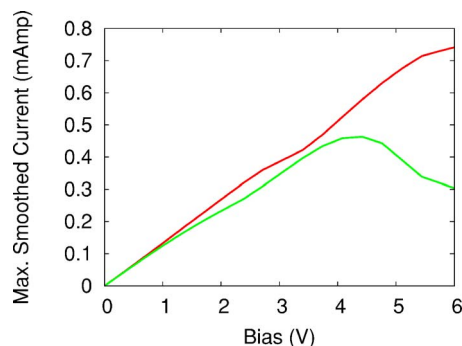


FIG. 9. (Color online) Maximum smoothed current through the central four carbons in $C_{50}H_{52}$ as a function of chemical potential bias (red line) and voltage bias (green). The results are quite similar until 4 V, at which point the bias is so large that the finite width of the valence band for polyacetylene causes the conductance to plateau in the voltage biased case.

the current apparently approach a constant value rather than falling to zero (see Fig. 10). This fact indicates that these fluctuations are characteristic of some physical current noise in the wire. We can easily quantify this noise from the transient current traces shown in Fig. 10 by simply computing the statistical uncertainty

$$S(V) = \int \langle \hat{I}(t) - \bar{I} \rangle^2 dt, \quad (21)$$

where \bar{I} is the average current for the given voltage and the integration runs over the quasisteady state currents shown in Fig. 10. We find that it is somewhat more difficult to converge the noise than the conductance—somewhat longer time windows, and hence somewhat longer wires, are required to obtain accurate noise compared to the conductance. This is consistent with the experimental situation, where successively higher moments of the electron counting distribution are progressively more difficult to obtain.⁸⁸ However, if we average over a window of 70 a.u. (≈ 1.7 fs), we obtain reasonably stable results for the noise in $C_{100}H_{102}$, as shown in Fig. 11. Clearly the noise increases linearly with increasing current, but the slope is much less than 1, indicating a

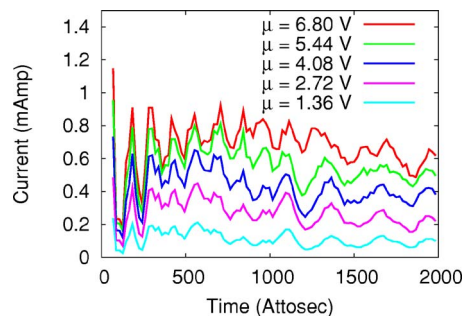


FIG. 10. (Color online) Transient current through the central four carbons in $C_{100}H_{102}$ at a series of different chemical potential biases. The current fluctuations previously observed with smaller reservoirs in $C_{50}H_{52}$ persist and are therefore not associated with a finite size effect.

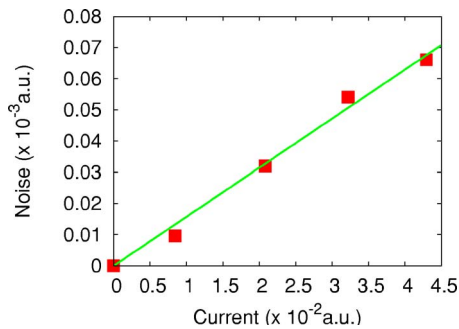


FIG. 11. (Color online) Statistical noise in the current through the central four carbons in $C_{100}H_{102}$. The data (squares) can be fit to a sub-Poissonian distribution (line).

sub-Poissonian process. It is not clear what the origin of this noise is. It may be that the application of the bias leads to a finite population of one or more molecular excited states which then keeps the system from relaxing to a steady state. Alternatively, this could be the result of the interference of incoming and outgoing waves within the molecule. We have not successfully isolated the origin of these fluctuations, and a case can be made for either picture.

Even without a molecular interpretation, the noise does give us some important clues about real-time transport simulations. There is a large body of work that discusses the rich history of conductance noise in quantum transport.^{84–91} In particular shot noise describes the instantaneous, quantum fluctuations of the current about its mean value

$$S \equiv \int \langle [I(t) - \bar{I}]^2 \rangle, \quad (22)$$

where the average $\langle \dots \rangle$ is taken over a time long compared to the characteristic time $\tau_0 \equiv e/\bar{I}$. Despite the mathematical similarity, the temporal noise [Eq. (21)] is not shot noise [Eq. (22)]. Shot noise arises from quantum uncertainty of the current for identically prepared systems, whereas our simulations reflect temporal uncertainty in the average current. However, for the ideal case of single-electron transport through a junction of transmittance T , the shot noise is also sub-Poissonian:^{84,85}

$$S \equiv e(1 - T)\bar{I}. \quad (23)$$

If we use this expression to fit the temporal noise in polyacetylene, we obtain $T \approx 0.98$, as compared to the numerically observed conductance of $0.8 G_0$. This discrepancy is to be expected on two grounds. First, because of the finite timestep, our simulations actually reflect the noise power over a particular interval rather than the noise itself. Second, shot noise involves two particle correlations while the noise we consider involves fluctuations in a one particle observable. These two quantities are in fact related via the fluctuation-dissipation theorem:¹¹⁵ by considering the response of the system to all possible potential perturbations, two particle observables such as $\langle \hat{I}^2 \rangle$ can be obtained without further approximation. By restricting ourselves to spatially uniform bias potentials, we recover only a fraction of the

associated fluctuations and observe an attendant reduction in the noise. Hence the analogy with shot noise can only be used for qualitative analysis of the temporal fluctuations in our simulations.

The important point about shot noise is that it becomes more prominent as the transmittance is reduced. This is, in fact, a generic property of noise—as the signal gets smaller noise become relatively more important. Hence, our results suggest that for molecular junctions—whose conductances are typically $0.01 G_0$ —temporal current noise will be a very significant factor. For example, in a purely metallic wire there is no shot noise in the large reservoir limit because it is a perfect conductor. This explains the observation that for a gold wire⁶⁵ the current-versus-time plots smoothly approach a plateau, while for polyacetylene, which only reduces the conductivity by 20%, noise already becomes important. Thus, it seems likely that the transient currents in a $0.01 G_0$ junction may be dominated by shot noise over quite large time intervals, making real-time simulations much more challenging.

CONCLUSIONS

In this article, we have demonstrated the feasibility of performing real-time TDDFT simulations of the transient current dynamics through a molecular wire at finite bias. These results were made possible by an efficient algorithm for integrating the TDKS equations in a localized basis that allows us to take very large time steps. Taking polyacetylene as our prototypical example, have shown that one can make a consistent definition of current and bias within TDDFT and obtain quantitative predictions of the current at finite bias by averaging the instantaneous current over a microscopic time window. Further, we have verified that these currents are converged with respect to the size of the reservoirs and that the results agree with the corresponding NEGF current-voltage character. Finally, we have investigated the temporal current noise and shown that for these wires, the noise does not decay to zero as the wire length is increased, but approaches a finite value. We argue that this noise is likely to be more significant in junctions that have low transmittance, which implies that real-time conductance simulations of MMM junctions—which have much lower transmittances than an isolated wire—may be quite challenging. In the near term, we plan to use TDDFT to study the conductance properties of some simple MMM junctions. The translation of this framework to such devices is straightforward in principle: one constructs a supersystem that contains enough metal atoms to mimic the “bulk” properties of the leads and propagates the system under an appropriate bias until a reliable average current can be extracted. Novel challenges that will need to be addressed for MMM junctions include the sensitivity of SCF convergence for metallic systems, the uncertain structure of the metal-molecule interface and the expected increase in noise due to the low transmittance of the junction. The points raised here—efficient integration of the TDKS equations, consistent definition of the bias potential, the importance of smoothing to obtain the relevant current—will facilitate study of these more technologically relevant devices.

For our time-dependent simulations, the average current provides an important validation of the model; by comparing to other predictions of the dc current, we can verify that our simulation is “large enough” and “long enough.” However, once the model has been validated, the average current is only one of a host of properties a real-time simulation gives access to. Electroluminescence, finite bias impedances, driven rectification and current triggered molecular dynamics can all be treated within the framework described here. Hence, this “microcanonical” picture of electron transport dynamics opens up a huge array of physical processes for theoretical study and we are currently in the process of analyzing some of these effects. In particular, it may be possible to predict the shot noise in a molecular junction without further approximation using TDDFT in conjunction with the fluctuation dissipation theorem.¹¹⁶

Finally, in regards to current voltage predictions, it has been pointed out that there are significant errors in the DFT currents at low bias due to improper cancellation between self-interaction errors⁶² and static electron correlation.^{44,51} We have shown that for time-independent problems, the balance between static correlation and self-interaction can be controlled by applying physically motivated constraints to the electron density.^{111–113} We are investigating ways in which this approach can be extended into the time domain to improve the transport predictions in real-time TDDFT.

ACKNOWLEDGMENTS

This work was supported by a CAREER award from the National Science Foundation (Grant No. CHE-0547877) and a grant from the NEC corporation.

-
- ¹T. A. Jung, J. K. Schlitler, J. K. Gimzewski, H. Tang, and C. Joachim, *Science* **271**, 181 (1996).
- ²L. A. Bumm, J. J. Arnold, M. T. Cygan, T. D. Dunbar, T. P. Burgin, L. Jones II, D. L. Allara, J. M. Tour, and P. S. Weiss, *Science* **271**, 1705 (1996).
- ³M. A. Reed, C. Zhou, C. J. Muller, T. P. Burgin, and J. M. Tour, *Science* **278**, 252 (1997).
- ⁴B. C. Stipe, M. A. Rezaei, and W. Ho, *Science* **280**, 1732 (1998).
- ⁵G. Leatherman, E. N. Durantini, D. Gust, T. A. Moore, A. L. Moore, S. Stone, Z. Zhou, P. Rez, and Y. Z. Liu, *J. Phys. Chem. B* **103**, 4006 (1999).
- ⁶H. Park, J. Park, A. K. L. Lim, E. H. Anderson, A. P. Alivisatos, and P. L. McEuen, *Nature (London)* **407**, 57 (2000).
- ⁷P. C. Collins, M. S. Arnold, and P. Avouris, *Science* **292**, 706 (2001).
- ⁸X. D. Cui, A. Primak, X. Zarate, J. Tomfohr, O. F. Sankey, A. L. Moore, T. A. Moore, D. Gust, and G. Harris, *Science* **294**, 571 (2001).
- ⁹P. L. McEuen, M. S. Fuhrer, and H. K. Park, *IEEE Trans. Nanotechnol.* **1**, 78 (2002).
- ¹⁰W. J. Liang *et al.*, *Nature (London)* **417**, 725 (2002).
- ¹¹J. Park *et al.*, *Nature (London)* **417**, 722 (2002).
- ¹²P. Avouris, *Acc. Chem. Res.* **35**, 1026 (2002).
- ¹³J. G. Kushmerick, J. Lazorek, C. H. Patterson, R. Shashidhar, D. S. Seferos, and G. C. Bazan, *Nano Lett.* **4**, 639 (2004).
- ¹⁴X. Y. Xiao, N. J. Xu, and B. Q. Tao, *Nano Lett.* **4**, 267 (2004).
- ¹⁵N. P. Guisinger, M. E. Greene, R. Basu, A. S. Baluch, and M. C. Hersam, *Nano Lett.* **4**, 55 (2004).
- ¹⁶R. L. McCreery, *Chem. Mater.* **16**, 4477 (2004).
- ¹⁷K. Kitagawa, T. Morita, and S. Kimura, *J. Phys. Chem. B* **109**, 13906 (2005).
- ¹⁸R. P. Andres, T. Bein, M. Dorogi, S. Feng, J. I. Henderson, C. P. Kubiak, W. Mahoney, R. G. Osifchin, and R. Reifenberger, *Science* **272**, 1323 (1996).
- ¹⁹R. Martel, T. Schmidt, H. R. Shea, T. Hertel, and P. Avouris, *Appl. Phys. Lett.* **73**, 2447 (1998).
- ²⁰J. Chen, M. A. Reed, A. M. Rawlett, and J. M. Tour, *Science* **286**, 1550 (1999).
- ²¹M. C. Hersam, N. P. Guisinger, J. Lee, K. Cheung, and J. W. Lydig, *Appl. Phys. Lett.* **80**, 201 (2002).
- ²²G. V. Nazin, D. L. Wang, and W. Ho, *Science* **302**, 77 (2003).
- ²³A. Salomon, D. Cahen, S. Lindsay, J. Tomfohr, V. B. Engelkes, and C. D. Frisbie, *Adv. Mater. (Weinheim, Ger.)* **15**, 1881 (2003).
- ²⁴D. L. Gittins, D. Bethell, D. J. Schiffrin, and R. J. Nichols, *Nature (London)* **408**, 67 (2000).
- ²⁵A. Aviram and M. Ratner, *Chem. Phys. Lett.* **29**, 277 (1974).
- ²⁶F. L. Carter, *Molecular Electronic Devices* (Marcel Dekker, New York, 1982).
- ²⁷C. Joachim, J. K. Gimzewski, and A. Aviram, *Nature (London)* **408**, 541 (2000).
- ²⁸R. Landauer, *IBM J. Res. Dev.* **1**, 223 (1957).
- ²⁹R. Landauer, *Philos. Mag.* **21**, 863 (1970).
- ³⁰R. Landauer, *Z. Phys. B* **21**, 247 (1975).
- ³¹M. Büttiker, *Phys. Rev. Lett.* **57**, 1761 (1986).
- ³²M. Büttiker, *Phys. Rev. B* **38**, 9375 (1988).
- ³³N. D. Lang, *Phys. Rev. B* **52**, 5335 (1995).
- ³⁴N. D. Lang, *Phys. Rev. Lett.* **79**, 1357 (1997).
- ³⁵N. D. Lang and P. Avouris, *Phys. Rev. Lett.* **81**, 3515 (1998).
- ³⁶E. G. Emberly and G. Kirczenow, *Phys. Rev. B* **58**, 10911 (1998).
- ³⁷J. Tomfohr and O. F. Sankey, *J. Chem. Phys.* **120**, 1542 (2004).
- ³⁸L. P. Kadanoff and G. Baym, *Quantum Statistical Mechanics* (Benjamin/Cummings, New York, 1962).
- ³⁹V. Mujica, M. Kemp, and M. A. Ratner, *J. Chem. Phys.* **101**, 6849 (1994).
- ⁴⁰M. P. Samanta, W. Tian, S. Datta, J. I. Henderson, and C. P. Kubiak, *Phys. Rev. B* **53**, R7626 (1996).
- ⁴¹L. E. Hall, J. R. Reimers, N. S. Hush, and K. Silverbrook, *J. Chem. Phys.* **112**, 1510 (2000).
- ⁴²S. Datta, *Superlattices Microstruct.* **28**, 253 (2000).
- ⁴³T. N. Todorov, *J. Phys.: Condens. Matter* **14**, 3049 (2002).
- ⁴⁴P. Delaney and J. C. Greer, *Phys. Rev. Lett.* **93**, 036805 (2004).
- ⁴⁵J. Taylor, H. Guo, and J. Wang, *Phys. Rev. B* **63**, 245407 (2001).
- ⁴⁶P. A. Derosa and J. M. Seminario, *J. Phys. Chem. B* **105**, 471 (2001).
- ⁴⁷Y. Xue, S. Datta, and M. A. Ratner, *Chem. Phys.* **281**, 151 (2002).

- ⁴⁸M. Brandbyge, J. L. Mozos, P. Ordejón, J. Taylor, and K. Stokbro, *Phys. Rev. B* **65**, 165401 (2002).
- ⁴⁹S. H. Ke, H. U. Baranger, and W. Yang, *Phys. Rev. B* **70**, 085410 (2004).
- ⁵⁰T. Tada, M. Kondo, and K. Yoshizawa, *J. Chem. Phys.* **121**, 8050 (2004).
- ⁵¹G. C. Solomon, J. R. Reimers, and N. S. Hush, *J. Chem. Phys.* **121**, 6615 (2004).
- ⁵²G. C. Solomon, J. R. Reimers, and N. S. Hush, *J. Chem. Phys.* **122**, 224502 (2005).
- ⁵³V. Mujica, M. Kemp, A. Roitberg, and M. A. Ratner, *J. Chem. Phys.* **104**, 7296 (1996).
- ⁵⁴H. Ness and A. J. Fisher, *Phys. Rev. Lett.* **83**, 452 (1999).
- ⁵⁵T. Kostyrko and B. R. Bulka, *Phys. Rev. B* **67**, 205331 (2003).
- ⁵⁶E. Runge and E. K. U. Gross, *Phys. Rev. Lett.* **52**, 997 (1984).
- ⁵⁷M. Petersilka, U. J. Gossmann, and E. K. U. Gross, *Phys. Rev. Lett.* **76**, 1212 (1996).
- ⁵⁸G. Stefanucci and C. O. Almbladh, *Europhys. Lett.* **67**, 14 (2004).
- ⁵⁹K. Burke, R. Car, and R. Gebauer, *Phys. Rev. Lett.* **94**, 146803 (2005).
- ⁶⁰M. Di Ventra and T. N. Todorov, *J. Phys.: Condens. Matter* **16**, 8025 (2004).
- ⁶¹N. Sai, M. Zwolak, G. Vignale, and M. Di Ventra, *Phys. Rev. Lett.* **94**, 186810 (2005).
- ⁶²C. Toher, A. Filippetti, S. Sanvito, and K. Burke, *Phys. Rev. Lett.* **95**, 146402 (2005).
- ⁶³R. Baer, T. Seideman, S. Ilani, and D. Neuhauser, *J. Chem. Phys.* **120**, 3387 (2004).
- ⁶⁴S. Kurth, G. Stefanucci, C. O. Almbladh, A. Rubio, and E. K. U. Gross, *Phys. Rev. B* **72**, 035308 (2005).
- ⁶⁵N. Bushong, N. Sai, and M. Di Ventra, *Nano Lett.* **5**, 2569 (2005).
- ⁶⁶X. F. Qian, J. Li, X. Lin, and S. Yip, *Phys. Rev. B* **73**, 035408 (2006).
- ⁶⁷K. Yabana and G. F. Bertsch, *Phys. Rev. B* **54**, 4484 (1996).
- ⁶⁸K. Yabana and G. F. Bertsch, *Int. J. Quantum Chem.* **75**, 55 (1999).
- ⁶⁹F. Calvayrac, P. G. Reinhard, E. Suraud, and C. A. Ullrich, *Phys. Rep.* **337**, 493 (2000).
- ⁷⁰K. Tada and K. Watanabe, *Phys. Rev. Lett.* **88**, 127601 (2002).
- ⁷¹M. A. L. Marques, X. Lopez, D. Varsano, A. Castro, and A. Rubio, *Phys. Rev. Lett.* **90**, 258101 (2003).
- ⁷²O. Sugino and Y. Miyamoto, *Phys. Rev. B* **59**, 2579 (1999).
- ⁷³R. Baer and R. Gould, *J. Chem. Phys.* **114**, 3385 (2001).
- ⁷⁴A. Castro, M. A. L. Marques, and A. Rubio, *J. Chem. Phys.* **121**, 3425 (2004).
- ⁷⁵D. S. Kosov and J. C. Greer, *Phys. Lett. A* **291**, 46 (2001).
- ⁷⁶D. S. Kosov, *J. Chem. Phys.* **120**, 7165 (2004).
- ⁷⁷D. S. Kosov, *J. Chem. Phys.* **119**, 1 (2003).
- ⁷⁸J. P. Perdew, R. G. Parr, M. Levy, and J. L. Balduz, Jr., *Phys. Rev. Lett.* **49**, 1691 (1982).
- ⁷⁹J. P. Perdew and M. Levy, *Phys. Rev. Lett.* **51**, 1884 (1983).
- ⁸⁰L. J. Sham and M. Schluter, *Phys. Rev. Lett.* **51**, 1888 (1983).
- ⁸¹H. Appel, E. K. U. Gross, and K. Burke, *Phys. Rev. Lett.* **90**, 043005 (2003).
- ⁸²A. D. Becke, *J. Chem. Phys.* **98**, 5648 (1993).
- ⁸³R. Gebauer, S. Piccinin, and R. Car, *ChemPhysChem* **6**, 1727 (2005).
- ⁸⁴V. K. Khlus, *Sov. Phys. JETP* **66**, 1243 (1987).
- ⁸⁵G. B. Lesovik, *JETP Lett.* **49**, 592 (1989).
- ⁸⁶C. W. J. Beenakker and M. Büttiker, *Phys. Rev. B* **46**, 1889 (1992).
- ⁸⁷M. Büttiker, *Phys. Rev. B* **46**, 12485 (1992).
- ⁸⁸L. S. Levitov and G. B. Lesovik, *JETP Lett.* **58**, 230 (1993).
- ⁸⁹M. Reznikov, M. Heiblum, H. Shtrikman, and D. Mahalu, *Phys. Rev. Lett.* **75**, 3340 (1995).
- ⁹⁰A. Kumar, L. Saminadayar, D. C. Glattli, Y. Jin, and B. Etienne, *Phys. Rev. Lett.* **76**, 2778 (1996).
- ⁹¹C. W. J. Beenakker, *Rev. Mod. Phys.* **69**, 731 (1997).
- ⁹²E. K. U. Gross, J. F. Dobson, and M. Petersilka, *Top. Curr. Chem.* **181**, 81 (1996).
- ⁹³E. K. U. Gross, J. F. Dobson, and M. Petersilka, *Top. Curr. Chem.* **181**, 81 (1996).
- ⁹⁴S. Bonella and D. F. Coker, *J. Chem. Phys.* **114**, 7778 (2001).
- ⁹⁵T. L. Gilbert, *Phys. Rev. B* **12**, 2111 (1975).
- ⁹⁶R. A. Donnelly and R. G. Parr, *J. Chem. Phys.* **69**, 4431 (1978).
- ⁹⁷R. Baer and M. Head-Gordon, *Phys. Rev. Lett.* **79**, 3962 (1997).
- ⁹⁸W. Kohn, *Phys. Rev. Lett.* **76**, 3168 (1996).
- ⁹⁹P. E. Maslen, C. Ochsenfeld, C. A. White, M. S. Lee, and M. Head-Gordon, *J. Phys. Chem. A* **102**, 2215 (1998).
- ¹⁰⁰M. Challacombe, *Comput. Phys. Commun.* **128**, 93 (2000).
- ¹⁰¹W. Magnus, *Commun. Pure Appl. Math.* **7**, 649 (1954).
- ¹⁰²S. Blanes, F. Casas, and J. Ros, *Numer. Math.* **40**, 434 (2000).
- ¹⁰³S. Blanes, F. Casas, J. A. Oteo, and J. Ros, *J. Phys. A* **31**, 259 (1998).
- ¹⁰⁴Wolfram Research, Inc., *MATHEMATICA*, Version 5.2 (Wolfram Research, Champaign, IL, 2005).
- ¹⁰⁵High Performance Computational Chemistry Group, *NWChem, A Computational Chemistry Package for Parallel Computers*, Version 4.6 (Pacific Northwest National Laboratory, Richland, Washington, 2004).
- ¹⁰⁶P. C. Hariharan and J. A. Pople, *Theor. Chim. Acta* **28**, 213 (1973).
- ¹⁰⁷M. Di Ventra and N. D. Lang, *Phys. Rev. B* **65**, 045402 (2001).
- ¹⁰⁸I. V. Ovchinnikov and D. Neuhauser, *J. Chem. Phys.* **122**, 024707 (2005).
- ¹⁰⁹P. O. Löwdin, *J. Chem. Phys.* **18**, 365 (1950).
- ¹¹⁰E. R. Davidson, *J. Chem. Phys.* **46**, 3320 (1967).
- ¹¹¹Q. Wu and T. Van Voorhis, *Phys. Rev. A* **72**, 024502 (2005).
- ¹¹²Q. Wu and T. Van Voorhis, *J. Chem. Theory Comput.* (to be published).
- ¹¹³I. Rudra, Q. Wu, and T. Van Voorhis, *J. Chem. Phys.* **24**, 024103 (2006).
- ¹¹⁴M. Kindermann, Y. V. Nazarov, and C. W. J. Beenakker, *Phys. Rev. Lett.* **90**, 246805 (2003).
- ¹¹⁵A. L. Fetter and J. D. Walecka, *Quantum Theory of Many-Particle Systems* (McGraw-Hill, New York, 1971).
- ¹¹⁶F. Furche and T. Van Voorhis, *J. Chem. Phys.* **122**, 164106 (2005).